RESEARCH ARTICLE | SEPTEMBER 21 2012

Wave packet calculations on nonadiabatic effects for the $O(^3P)+HF(^1\Sigma^+)$ reaction under hyperthermal conditions

S. Gómez-Carrasco; N. Bulut; L. Bañares; O. Roncero

J. Chem. Phys. 137, 114309 (2012)
https://doi.org/10.1063/1.4753811

Wave packet calculations on nonadiabatic effects for the $O(^3P)+HF(^1\Sigma^+)$ reaction under hyperthermal conditions

S. Gómez-Carrasco,[1] N. Bulut,[2] L. Bañares,[3] and O. Roncero[4,a)]
[1]*Departamento de Química Física, Facultad de Ciencias Químicas, Universidad de Salamanca, Plaza de los Caídos s/n, 37008 Salamanca, Spain*
[2]*Department of Physics, Firat University, 23169 Elazig, Turkey*
[3]*Departamento de Química Física I, Facultad de Ciencias Químicas, and Unidad Asociada de I+D+i al Consejo Superior de Investigaciones Científicas, Universidad Complutense de Madrid, 28040 Madrid, Spain*
[4]*Instituto de Física Fundamental, CSIC, C/ Serrano 123, 28006 Madrid, Spain*

(Received 18 July 2012; accepted 4 September 2012; published online 21 September 2012)

We present wave packet calculations of total and state-to-state reaction probabilities and integral cross sections for the nonadiabatic dynamics of the $O(^3P)+HF \rightarrow F(^2P)+OH(^2\Pi)$ reaction at hyperthermal collision energies ranging from 1.2 to 2.4 eV. The validity of the centrifugal sudden approximation is discussed for the title reaction and a comprehensive investigation of the influence of nonadiabatic effects on the dynamics of this reactive system at high (hyperthermal) collision energies is presented. In general, nonadiabatic effects are negligible for averaged observables, such as total reaction probabilities and integral cross sections, but they are clearly observed in detailed observables such as rotationally state-resolved reaction probabilities. A critical discussion of nonadiabatic effects on the dynamics of the title reaction is carried out by comparing with the reverse reaction and the characteristics of the adiabatic and diabatic potential energy surfaces involved. © *2012 American Institute of Physics*. [http://dx.doi.org/10.1063/1.4753811]

I. INTRODUCTION

Recent experimental and theoretical research on reaction dynamics has focused on deciphering the mechanism of high-energy or hyperthermal collisions that take place in extreme environments, such as those occurring in the region of spacecrafts-atmosphere interaction. Actually, this has become an essential topic in spacecraft system engineering.[1,2] The most abundant component of the atmosphere below 800 km is atomic oxygen, a strong oxidizing agent, and, as a consequence, this species at hyperthermal velocities is one of the main sources of erosion of the spacecrafts surface. Therefore, the reactivity of hyperthermal atomic oxygen $O(^3P)$ has generated a particular interest and the need of understanding its chemistry at these extreme conditions has become recently a new topic in reaction dynamics, both experimentally and theoretically.

On the experimental side, the research done by Minton and co-workers on the reactivity of hyperthermal atomic oxygen with a great variety of molecules, such as CO,[3] H_2O,[4] and HCl[5–8] or supramolecular systems, such as polymers,[9] hydrocarbon surfaces,[10] or ionic liquid surfaces,[11] is worth noting. On the theoretical side, most of the calculations at hyperthermal energies have been developed parallel to the experimental research and they have consisted mainly on on-the-fly quasi-classical trajectories (QCT) calculations using semiempirical methods for the calculation of the potential energy and gradients.[5,7,12] To our knowledge no quantum dynamics method has been applied yet to study these reactive systems at very high collision energies and this is the main reason of the present work, where converged nonadiabatic wave packet calculations have been carried out for the title reaction.

In contrast to reactions in thermal conditions, some interesting energetic and dynamical features of reactive collisions emerge under hyperthermal conditions. New reaction channels appear since the available energy is significantly large, and reaction may occur following unexplored mechanisms. For example, it has been recently observed experimentally by Zhang *et al.*[5,8] that for the $O(^3P)+HCl$ reaction at hyperthermal collision energies, endothermic channels (OCl+H) can become dominant with respect to lowest-lying reaction paths (OH+Cl). With this experiment in mind, Binder *et al.*[7] analyzed theoretically the effect of including excited electronic states on the OCl/OH branching ratio for the $O(^3P)+HCl \rightarrow OCl+H$ reaction by means of QCT calculations. An important increase of the OCl/OH ratio with increasing collision energy was found, concluding that excited electronic states can enhance a particular reaction channel under hyperthermal conditions. Although this result emphasizes the need of including excited electronic states in the calculations, the role of nonadiabatic effects under hyperthermal conditions has not been explored yet and this will be one of the aims of the present work.

This work focuses on the $O(^3P)+HF \rightarrow F(^2P)+OH(^2\Pi)$ reaction at high collision energies from threshold up to 2.4 eV. Neglecting spin-orbit effects, 12 electronic states in the $C_{\infty v}$ symmetry group correlate asymptotically with the $F(^2P)+OH(^2\Pi)$ channel. Among them, three triplet states (the $^3\Sigma^-$ and $^3\Pi$ states) and five singlet states (the $^1\Delta$, $^1\Pi$, and $^1\Sigma^+$ states) connect the $O(^3P)+HF$ and $O(^1D)+HF$ asymptotes, respectively. The other three remaining electronic

a)Author to whom correspondence should be addressed. Electronic mail: octavio.roncero@csic.es.

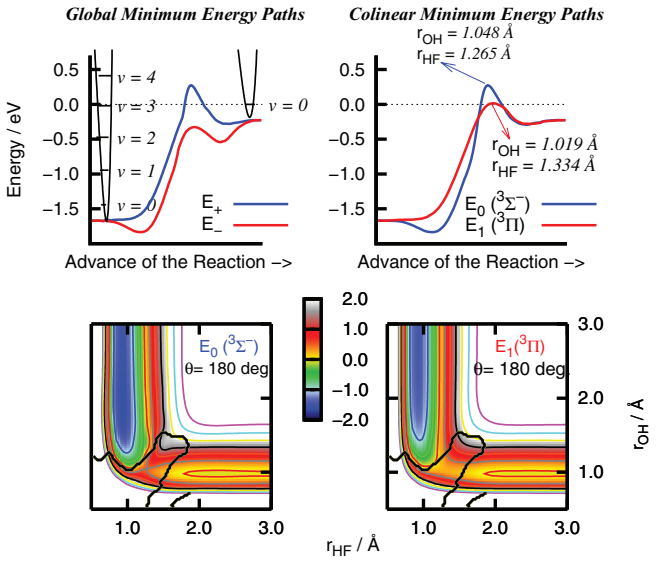

FIG. 1. (Top) Minimum energy path for the $O(^3P)$+HF reaction (in eV) for the two first energy roots; (left) for the adiabatic $1^3A''$ and $2^3A''$ states, denoted E_- and E_+, respectively, resulting from the regularized diabatic states of Ref. 26; (right) for the diabatic $^3\Sigma^-$ and $^3\Pi$ states (denoted E_0 and E_1) at a collinear geometry. (Bottom) Contour plots (in eV) of the two diabatic (left) $^3\Sigma^-$ and (right) $^3\Pi$ state at OHF collinear geometry, indicating with a line in black the conical intersection seams.

states correlate to excited electronic states of the HF diatom. Figure 1 shows the collinear minimum energy paths of the states mentioned above. In the last few years, global accurate three-dimensional adiabatic potential energy surfaces (PES's) have been obtained for all the triplet[13,14] and singlet[15] electronic states connecting the $O(^3P,^1D)$+HF asymptotes. On these potential energy surfaces, both reactivity[13,14,16–22] and spectroscopy[15,23–25] of the OHF system have been extensively studied. Note that, due to the large endoergicity of the $O(^3P)$+HF→$F(^2P)$+$OH(^2\Pi)$ reaction, the only studies carried out up to date on the triplet lowest-lying surfaces were performed for the reverse $F(^2P)$+OH→$O(^3P)$+HF reaction. Also, the dynamics of the $FO(^2\Pi)$+H→$OH(^2\Pi)$+$F(^2P)$ reaction on the ground triplet state ($1^3A''$) has been recently analyzed by means of both QCT[19,20] and quantum mechanical wave packet calculations.[18,19] Chu *et al.*[19,21] have also focused on the $OH(^2\Pi)$+$F(^2P)$ and $O(^1D)$+HF channels, on the triplets ($1^3A''$ and $1^3A'$) and singlet ($^1A'$) states, respectively. Later, a model of coupled diabatic PES's for the three lowest triplet electronic states has been also proposed,[26] what allows to study the influence of the nonadiabatic mechanisms on the dynamics of the system, mainly applied to the study of the photodetachment spectrum of the OHF^- anion.[26] Recently, state-to-state cross sections and specific rate constants have been calculated for the $F(^2P)$+OH→$O(^3P)$+HF reaction by Zanchet *et al.*[27] on these diabatic PES's.

The objective of the present work is to study the nonadiabatic dynamics of the $O(^3P)$+HF→$F(^2P)$+$OH(^2\Pi)$ reaction at collision energies in the range 1.2−2.4 eV. The dynamics of the system is followed using a time-dependent wave packet method and it will proceed on the already mentioned set of coupled diabatic PESs.

The paper is structured as follows: Section II describes the computational details, while Sec. III is devoted to the presentation of the most important results obtained in this work. Conclusions and suggestions for future work are finally presented in Sec. IV.

II. COMPUTATIONAL DETAILS

The state-to-state $O(^3P)$+$HF(^1\Sigma^+, v=0)$→$OH(^2\Pi, v', j')$+$F(^2P)$ reaction dynamics is studied using the coupled diabatic potential energy surfaces recently developed for this system by Gómez-Carrasco *et al.*[26] to account for the nonadiabatic transitions induced by the existing conical intersections (CIs). As can be seen in Fig. 1, these CIs appear near the transition state due to the crossing between the $^3\Pi$ and $^3\Sigma^-$ states at collinear geometries. The $^3\Sigma^-$ state presents two shallow wells at each side of the reaction barrier. The $^3\Pi$ state presents the lowest reaction barrier and no well at the entrance channel. The resulting ground adiabatic state presents a low reaction barrier, lower than for any diabatic state due to the $\Sigma - \Pi$ interaction, and it appears at a bent geometry.

The reverse reactive collisions were studied on these surfaces by Zanchet *et al.*[27] It was found that important nonadiabatic transitions take place in the dynamics, yielding a significant increase of the reaction cross sections and rate constants. Spin-orbit splittings of the $OH(^2\Pi)$+$F(^2P)$ reactants were also found to be very important, because the change of the electronic partition function yields an important increase of the rate constant, improving the agreement with the few experimental data available.[28] The role of spin-orbit couplings in producing transitions among the many spin-orbit states remains to be solved, since it requires the development of about 24 coupled spin-orbit states. The reaction under study is endoergic by ≈1.5 eV, as can be seen in Fig. 1, and the $O(^3P)$ spin-orbit splittings (158 and 227 cm^{-1}) will be neglected.

In the $O(^3P)$+$HF(^1\Sigma^+)$ channel, the diabatic states corresponds to an open-shell atom in a P state, while in the $OH(^2\Pi)$+$F(^2P)$ asymptote there are two open-shell fragments. A proper connection between the electronic states in the two rearrangement channels would imply a more complete diabatic representation, in which all the states correlating to each of the electronic states of the two asymptotes are considered separately. Such a representation would imply (without spin-orbit coupling) three triplet states in the $O(^3P)$+$HF(^1\Sigma^+)$ asymptote and six triplet states in the $OH(^2\Pi)$+$F(^2P)$ channels, which is out of the scope of this work. To simplify, we shall model the system as a closed-shell diatomic molecule (in the two rearrangement channels) plus an P open-shell atom, whose states are designated by Λ, the projection of the electronic orbital angular momentum along the z axis. There are three states with $\Lambda = 0,\pm1$. When the symmetry under reflexion of the xz body-fixed plane is considered, the $\Lambda = +1$ and -1 combine to give two symmetry adapted states, one in and one out of the molecular plane, of A'' and A' symmetry, respectively. The $^3A'$ corresponds exactly to the adiabatic state calculated previously[14] and presents the highest reaction barrier. Since this state yields low reaction probabilities, it will be neglected and only

the two states of $^3A''$ symmetry, with higher reactivity, will be considered hereafter, either in the adiabatic or the diabatic representations.

The closed-shell molecule plus open-shell atom is described by the Hamiltonian of Rebentrost and Lester.[29] In the present work, in the adiabatic representation (obtained by diagonalizing the 2×2 diabatic matrix) the electronic orbital angular momentum is neglected (or set to zero), while in the diabatic representation, two states with $\Lambda = 0$ and 1 are considered. The diabatic $\Lambda = 0$ (or $^3\Sigma^-$) state presents the same states than in the adiabatic representation, and for initial $j = 0$ reactants only the parity, ϵ, equal to $(-1)^J$ exists. For the $\Lambda = 1$ (or $^3\Pi$), the situation changes for initial $j = 0$: there is no physical state for $J = 0$, while for $J > 0$ the two parities, $\epsilon = \pm 1$, exist, corresponding to the two projections of Λ. These two projections correspond to the $^3A''$ and $^3A'$ adiabatic states, and in the present case we keep the linear combination of $^3A''$ symmetry, neglecting the other corresponding to the $^3A'$. The effect of this situation will be discussed below.

The state-to-state reaction probabilities are calculated using a wave packet method, with the code MADEWAVE3 recently reported.[30] For this HL+H′→H+LH′ mass combination (where H and L stand for heavy and light atoms, respectively), the principal axis of inertia coincides approximately with the H-H′ internuclear vector, and this vector is very close to **R** and **R**′, the Jacobi vectors joining the diatomic center-of-mass (HF or OH, for reactants or products, respectively) to the atomic fragment. For this reason, product Jacobi coordinates are more efficient in this case.[31] The parameters used in the propagation are listed in Table I. Due to the mass combination and the high kinetic energies involved, it is necessary to use dense grids. In particular, to get a good convergence it is necessary to use about 280 angular points, and describe adequately the F+OH channel at long distances, which requires Jacobi angles γ' close to collinear geometries. The calculations become very heavy computationally, and are performed by parallelization in the number of angular grid points and the helicities, Ω, considered in the calculation for $J > 0$. In the present calculations, the initial wave packet is located in the asymptotic reactant channel, where there is no influence of the interaction potential, and the propagation grid scheme is defined using the product Jacobi coordinates. In order to calculate the reaction probabilities, it is necessary to integrate the initial wave packet flowing into the possible channels. The calculations are carried out with the same parameters for each adiabatic and diabatic surfaces.

TABLE I. Parameters used in the wave packet calculations in product Jacobi coordinates. Distances are in Å, and energies in eV.

r_{min} (Å)	0.4
r_{max} (Å)	13
N_r	256
r_I (Å)	11
A_r (Å^{-2})	0.01
R_{min} (Å)	0.4
R_{max} (Å)	13
N_R	512
R_I (Å)	11
A_R (Å^{-2})	0.035
N_γ	280 in $[0, \pi]$
R_0 (Å)	10
E_0 (eV)	2
ΔE (eV)	.25
R'_∞	9
V_{cut} (eV)	4
E^{ℓ}_{cut} (eV)	5

The calculation of the integral cross sections as a function of collision energy for each ro-vibrational state v, j of the reagent molecule, $\sigma_{v,j}(E_c)$, requires summing up the contributions from all possible values of the total angular momentum J,

$$\sigma_{vj}(E_c) = \frac{\pi}{k^2}\frac{1}{2j+1}\sum_{J=0}^{J_{max}}(2J+1)[2\min(J,j)+1]P^J_{vj}(E_c), \tag{1}$$

where $k^2 = 2\mu_r E_c/\hbar^2$, and $P^J_{v,j}(E_c)$ is the reaction probability from the initial rovibrational state v, j summed over all final states as a function of collision energy, E_c, at a total angular momentum J, which can be written in terms of the S matrix elements as

$$P^J_{vj}(E_c) = \frac{1}{2\min(J,j)}\sum_{\Omega}\sum_{\Omega',v',j'}|S^J_{v',j',\Omega',v,j,\Omega}|^2. \tag{2}$$

Centrifugal sudden (CS) calculations, including only $\Omega = 0$, and close-coupling (CC) calculations, including several Ω projections, on the adiabatic and diabatic states have been performed for selected total angular momenta, $J = 0$, 10, 20, 30, 40, …, 140, with a step of 10, which are necessary for convergence of cross sections up to 2.4 eV including eight helicity components, $\Omega = 0, \ldots, 7$. Intermediate total angular momenta or partial waves are obtained by an interpolation procedure based on the J-shifting approach. With this approach for a given J value $J \in [J_1, J_2]$, the reaction probability is obtained as

$$P_J(E) = \frac{J-J_1}{J_2-J1}P_{J_1}(E - B[J(J+1) - J_1(J_1+1)]) + \frac{J_2-J}{J_2-J1}P_{J_2}(E + B[J_2(J_2+1) - J(J+1)]), \tag{3}$$

where E is the total energy and the rotational constant B is previously fitted. This way, the total integral cross sections are obtained by using Eq. (1).

III. RESULTS AND DISCUSSION

A. Reaction probabilities

Total reaction probabilities as a function of collision energy for total angular momentum $J = 0$ for the different adiabatic and diabatic states and the corresponding sums are depicted in Figure 2. The reaction probabilities obtained in the diabatic and adiabatic representations for those cases correlating asymptotically to the same state (i.e., $^3\Sigma^-$ and $1^3A''$, and $^3\Pi$ and $2^3A''$) are very similar. They all show a threshold

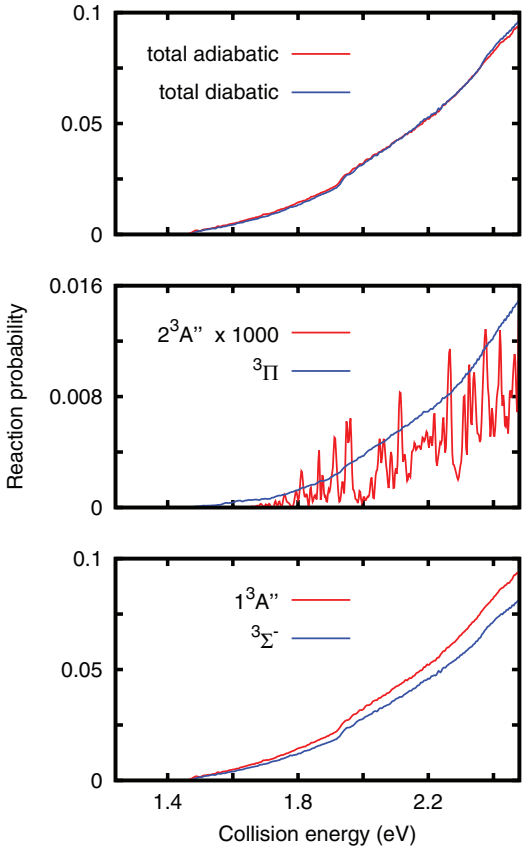

FIG. 2. Total reaction probabilities as a function of collision energy for the $O(^3P)$+HF($v = 0$, $j = 0$) reaction at total angular momentum $J = 0$. Top panel: sum over initial electronic states in the diabatic and adiabatic representations. Middle panel: comparison between the adiabatic $2^3A''$ probability and that obtained in the 2×2 diabatic representation starting in the $^3\Pi$ state. Bottom panel: The same but for the ground adiabatic $1^3A''$ state and for the initial diabatic $^3\Sigma$ state for each of the two diabatic electronic states (considering the 2×2 electronic diabatic Hamiltonian).

at ≈1.4 eV and a monotonic increase after threshold up to 2.4 eV collision energy. The reaction probability is of the same order in all cases, with the exception of the probability associated with the excited adiabatic $2^3A''$ state, which is considerably smaller (note that in the figure, this curve has been multiplied by a factor of 10^3). Additionally, this reaction probability shows significant structure associated with resonances. The $2^3A''$ state presents a higher barrier for reaction, and that is the reason for the higher threshold, located at 1.65 eV. However, the higher barrier cannot explain by itself the small values of the reaction probabilities that we attribute to the larger angular cone of acceptance of the ground electronic state. It is the $\Sigma - \Pi$ electronic interaction what produces a repulsion between the two diabatic electronic states, giving rise to a bent geometry of the saddle point for the ground electronic state. On the contrary, the resulting excited $2^3A''$ surface presents a higher saddle point at collinear geometry.

When considering the diabatic representation, the reaction shows about the same energy threshold for the two initial electronic states. Since they have different energy barriers (both at collinear geometry in the top right panel of Figure 1), this is a clear indication that electronic transitions occur. Otherwise, reaction on each surface should have presented significantly different thresholds. Moreover, the $^3\Pi$ state, having a somewhat higher threshold, it is also the one showing a lower reaction probability, about six times lower than that corresponding to the initial $^3\Sigma^-$ state. This is surprising since the $^3\Pi$ state presents a lower barrier. As indicated above, this can be explained considering the larger angular cone of acceptance of the surface of this state and the electronic transitions induced by the non-diagonal elements of the electronic diabatic matrix.

The differences between the diabatic and adiabatic representations are washed out when the reaction probabilities for the initial electronic states are summed. These sums are shown in the top panel of Figure 2, and are nearly indistinguishable. In contrast, in the reverse reaction, a difference of the order of 1/3 was found.[27] In that case, the initial translational energies were considerably lower, and the dynamics was much slower. Also, in the reverse process, the reaction probability showed resonances, specially at low energies near threshold. However, in the present reaction, the collision energy is much higher and the reaction probability does not show resonances, indicating a rather direct mechanism. This fast dynamics may explain why the sum of reaction probabilities at $J = 0$ in the diabatic and adiabatic representations is nearly the same, showing that the electronic transitions (not occurring in the adiabatic case) do not have a net effect on the total reaction probability summed over initial electronic states.

For these same reasons, the CS approximation is expected to work rather well for this reaction. The process seems to be direct and fast in the entrance channel, and the system passes rapidly through the interaction region, where the Coriolis couplings have larger effects. In addition, the light hydrogen atom is always attached to one of the heavier atoms, either F or O, so that the principal axis of inertia nearly coincides with the F-O internuclear vector, always close to the **R** and **R**′ vectors in reactant and product Jacobi coordinates. In order to check for the validity of the CS approximation, Figure 3 shows the comparison between the total reaction probabilities calculated on the two adiabatic electronic states for several J values using the CS approximation in reactant and product Jacobi coordinates, and an exact CC calculation. The CC calculation is performed with $\Omega_{max} = 7$ helicity projections in product Jacobi coordinates. The CS calculations only consider $\Omega = 0$ in the reactant and product frames. As can be seen, the two CS calculations are in good agreement with the CC results for all J values. A similar situation holds for the calculations performed on the coupled diabatic states (not shown). It seems that the CS approximation in product Jacobi coordinates yields slightly better results when compared with the CC calculation in all cases. This fact can be explained by considering that the slower dynamics, where Coriolis couplings are more efficient, occurs predominantly in that rearrangement channel.

Further insight into the dynamics of the title reaction is provided by the electronically and vibrationally state-resolved reaction probabilities as a function of collision energy at $J = 0$, which are displayed in Figure 4. The bottom panels show the vibrationally state-resolved reaction probabilities when

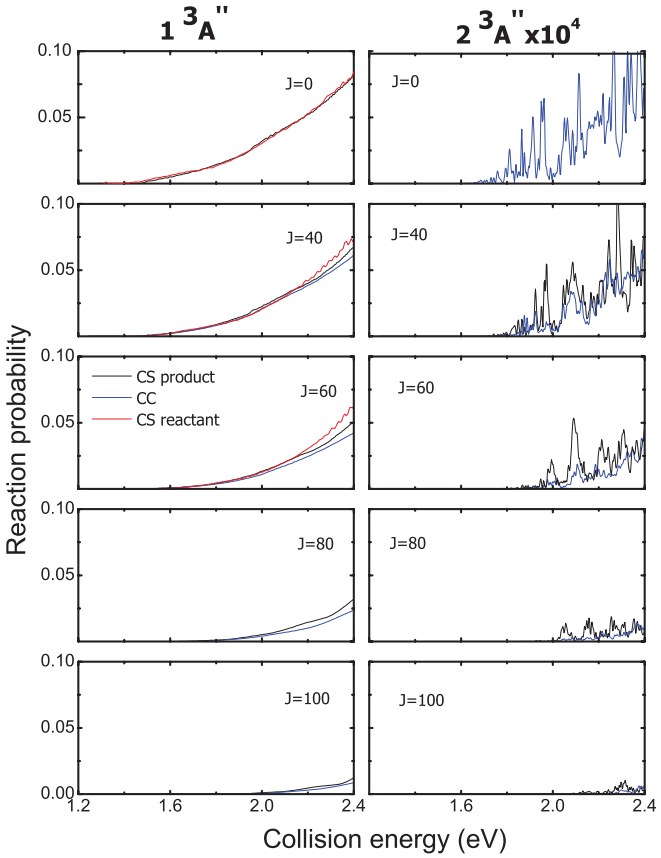

FIG. 3. Total reaction probabilities as a function of the collision energy calculated for the $O(^3P)$+HF($v = 0$, $j = 0$) reaction on the $1^3A''$ (left panels) and $2^3A''$ (right panels) initial adiabatic electronic states at several values of the total angular momentum J using the CS approximation in reactant (red) and product (black) Jacobi coordinates and the CC methodology (blue).

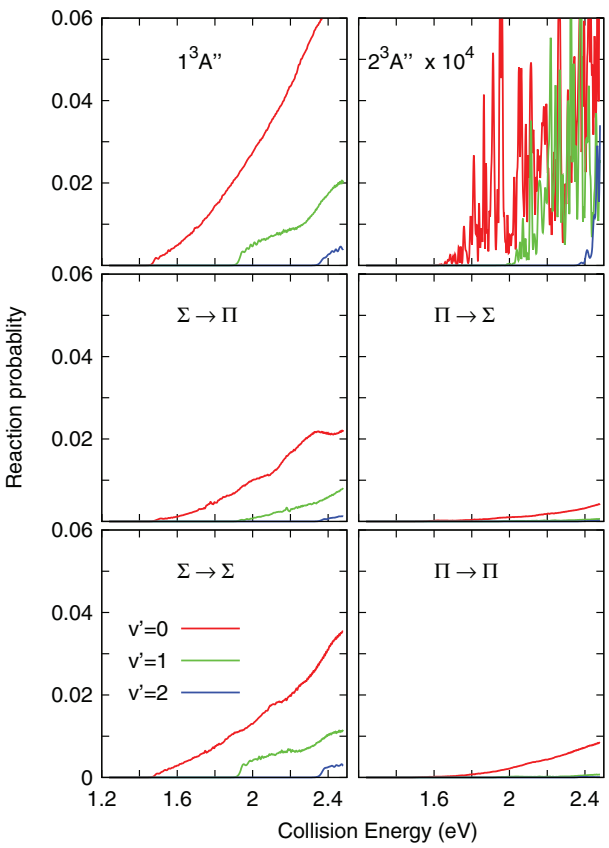

FIG. 4. Electronically and vibrationally state-resolved reaction probabilities as a function of collision energy for the $O(^3P)$+HF(α,$v = 0$, $j = 0$)→OH(α',$v' = 0$–2)+F reaction at $J = 0$. Bottom panels: ending in the same diabatic electronic state of the initial wave packet ($\alpha = \alpha' = {}^3\Sigma$ or ${}^3\Pi$). Middle panels: with different initial and final electronic state ($\alpha \neq \alpha'$). Top panels: obtained in the adiabatic representation for the $1^3A''$ (left) and $2^3A''$ (right) states.

reaction ends on the same diabatic electronic state than that where the wave packet was initially located, while in the middle panels the final electronic state differs from the initial one. The results indicate that the dynamics induces electronic transitions between the two diabatic states, since they cross at both sides of the saddle points. However, the sum over the initial and final electronic states is nearly the same as that obtained in the adiabatic representation. A similar situation was also found in the reverse reaction,[27] but in that case the total reaction probabilities were different as a function of energy, being higher at low energies and lower at high energies. In fact, at low energies there were many resonances, which are relatively long lived, which indicates that the system explores the region of the transition state with enough time to undergo several electronic transitions. In the present case, the dynamics is direct, and resonances do not seem to play an important role. Thus, when the system passes through the transition state, it may experience one or two electronic transitions, but without changing the total reaction probability. The final vibrational distribution is neither varied significantly with respect to the adiabatic calculations, which are also shown in the top panels of Figure 4.

The resonance structures found on the $2^3A''$ adiabatic state reaction probability calculations are not present in the ${}^3\Pi$ diabatic state (see Figures 2 and 4). The reason is that the reaction probability associated to the ${}^3\Pi$ state is larger, essentially due to direct reaction through nonadiabatic transitions, so that resonances become immersed in a large continuum background. Also, the two diabatic states present nearly the same threshold, while the two adiabatic states do not. These are the only aspects in which the electronic transitions can play a role, distinguishing the diabatic and adiabatic representations. Otherwise, the total or vibrationally state-resolved reaction probabilities summed over initial and final electronic states are nearly indistinguishable for the title reaction, which is not the case for the reverse reaction.[27]

In order to get clearer evidences of nonadiabatic dynamics, more detailed observables have to be analyzed. The rotational angular momentum is coupled to the orbital angular momentum and, therefore, final rotational distributions should be affected by nonadiabatic dynamics. Figure 5 shows rotationally state-resolved reaction probabilities as a function of collision energy for the $O(^3P)$+HF($v = 0$, $j = 0$) reaction at $J = 0$. Also in this case, a large transition probability in the diabatic representation is present, while in the adiabatic representation the $2^3A''$ reaction probabilities are almost negligible. The larger structures observed in the rotationally state-resolved reaction probabilities in comparison with the vibrationally state-resolved reaction probabilities can be explained

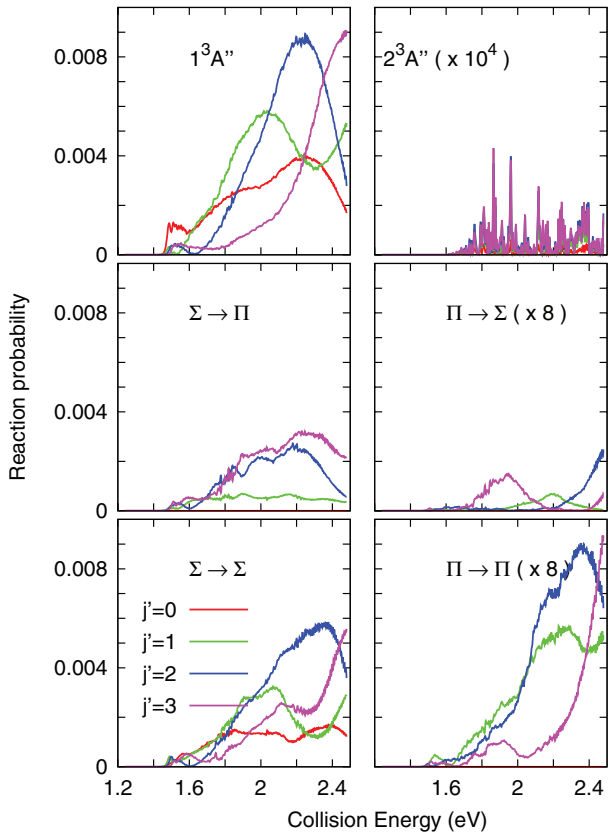

FIG. 5. Electronically and rotationally state-resolved reaction probabilities as a function of collision energy for the $O(^3P)$+HF(α,v = 0,j = 0)→OH(α',v' = 0,j' = 0–3)+F reaction at J = 0. Bottom panels: ending in the same diabatic electronic state of the initial wave packet ($\alpha = \alpha' = {}^3\Sigma$ or ${}^3\Pi$). Middle panels: with different initial and final electronic state ($\alpha \neq \alpha'$). Top panels: obtained in the adiabatic representation for the $1^3A''$ (left) and $2^3A''$ (right) states.

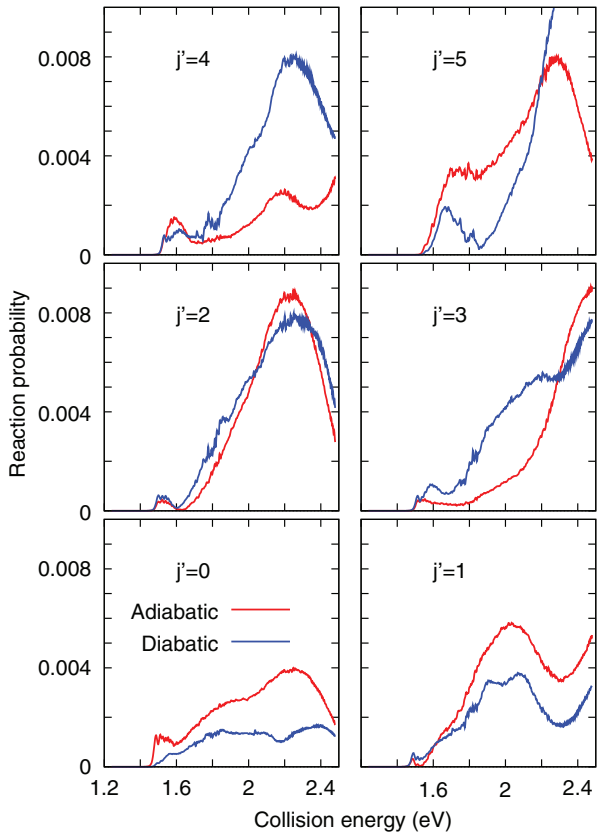

FIG. 6. Rotationally state-resolved reaction probabilities as a function of collision energy for the $O(^3P)$+HF(v = 0,j = 0)→OH(v' = 0,j' = 0–5)+F reaction at J = 0 calculated in the adiabatic (red) and diabatic (blue) representations.

by the fact that the bent character of the transition state causes some rotational excitation in the products. The sum over all initial and final electronic states, shown in Figure 6, indicates that the total rotational state-resolved cross sections are different in the diabatic and adiabatic representations. In fact, in the diabatic representation product rotation appears more excited. This difference is due to the coupling between electronic and rotational angular momenta, which is treated differently in the two representations. This fact can be considered as an evidence of nonadiabatic effects on the reaction dynamics of the title reaction.

B. Cross sections

Figure 7 shows integral cross sections as a function of collision energy for the $O(^3P)$+HF(v = 0, j = 0) reaction for the different adiabatic and diabatic states and the corresponding sums (bottom and middle panels, respectively). In all cases, the integral cross sections show a monotonous and smooth increase after a reaction threshold as collision energy increases. The only exception to the general behavior, typical of reactions with an energy barrier, is the integral cross section calculated on the adiabatic $2^3A''$ state, which shows some structure associated to resonances and it is significantly (about 10^4 times) smaller. The electronic transitions in the diabatic representation are depicted in the top panel of Figure 7, where the diagonal and non-diagonal integral cross sections for the two initial and final electronic states are represented. As can be seen, these electronic transitions have a non negligible cross section, being smaller for the ${}^3\Pi$ initial state than for the ${}^3\Sigma^-$ initial state. As in the case of reaction probabilities, the integral cross sections summed over the initial and final electronic states in both representations are practically indistinguishable. Thus, the total integral cross sections do not show any evidence of nonadiabaticity.

These results differ from those found for the reverse reaction,[27] in which the nonadiabatic dynamics in the diabatic representation yielded a small, but noticeable, integral cross section increase with respect to the pure adiabatic representation. As discussed above, this different behavior can be explained by the different "speed" of the dynamics: while for the title reaction, collision energy is large (above 1.5 eV), for the reverse reaction collision energies are considerable smaller (below 0.5 eV). This significant difference in collision energy implies that in the present case the reaction mechanism is rather direct, while for the reverse reaction, the collision process is indirect with the presence of many resonances. At short distances, the non-diagonal electronic and Coriolis terms are larger, yielding more efficient electronic and helicity transitions in the latter case.

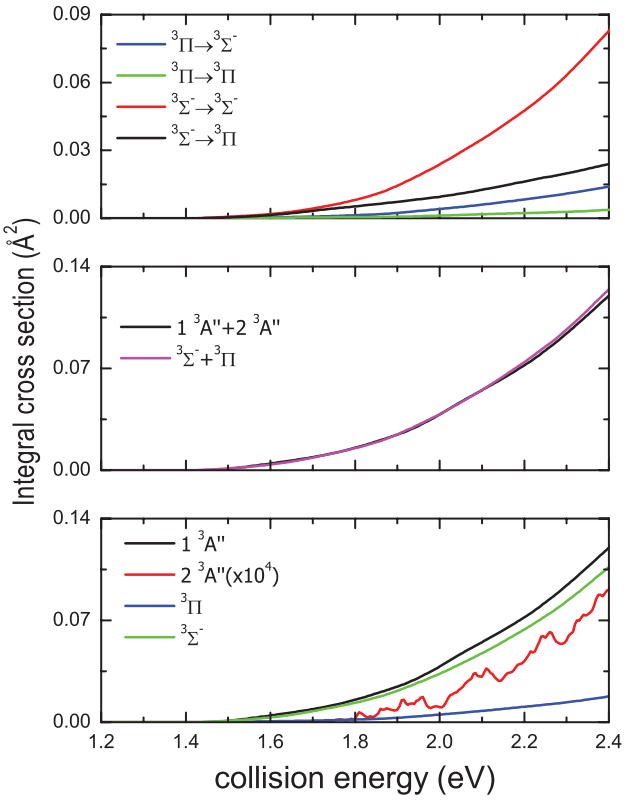

FIG. 7. Total integral cross sections as a function of collision energy for the $O(^3P) + HF(v = 0, j = 0) \rightarrow OH + F$ reaction in the adiabatic and diabatic representations. Bottom panel: obtained for the adiabatic $1^3A''$ and $2^3A''$ and diabatic $^3\Sigma^-$ and $^3\Pi$ states. Middle panel: total diabatic versus total adiabatic. Top panel: diagonal and nondiagonal cross sections obtained in the diabatic representation for the two initial and final electronic states.

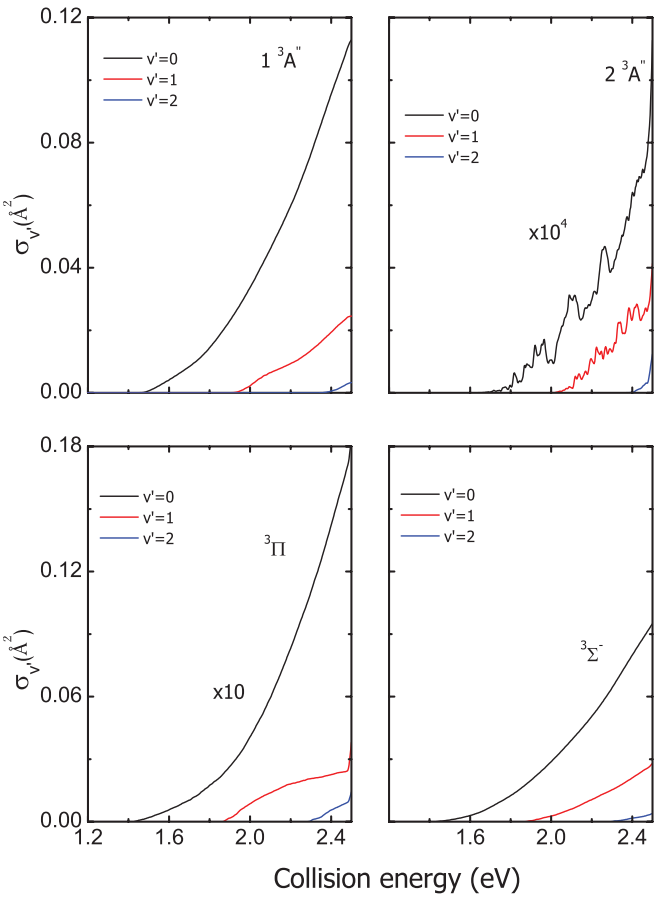

FIG. 8. Vibrationally state-resolved integral cross section as a function of collision energy for the $O(^3P)+HF(v = 0, j = 0) \rightarrow OH(v')+F$ reaction obtained for the $1^3A''$ and $2^3A''$ adiabatic states and for the $^3\Sigma^-$ and $^3\Pi$ coupled diabatic states as indicated. In the diabatic cases, the cross sections for the two possible final electronic states have been added.

The increase of the integral cross section for the reverse reaction was nevertheless not enough to reproduce the available experimental data. The inclusion of the spin-orbit splitting in the electronic partition function yielded a further increase in the rate constants. In the present case, at the high collision energies considered, because of the low splitting of the $O(^3P)$ levels, this effect is considered to be negligible. We, therefore, conclude that nonadiabatic effects are not important to reproduce the total integral cross section for the title reaction.

The vibrationally state-resolved integral cross sections as a function of collision energy are displayed in Figure 8 and show a similar behavior. In the collision energy range studied, only three product vibrational states ($v' = 0, 1, 2$) are formed. The magnitude of the product vibrationally state-resolved cross sections obtained on the adiabatic $1^3A''$ and diabatic $^3\Sigma^-$ states are very close to each other and are larger than those calculated on the adiabatic $2^3A''$ and diabatic $^3\Pi$ states. The cross sections calculated on the adiabatic $2^3A''$ state are very small (note that in the figure a factor of 10^4 is used) and do not contribute to the final vibrational distribution of products in the adiabatic representation.

Figure 9 shows product rotational distributions for different electronic and vibrational states obtained at several collision energies. As can be seen, irrespective of the initial electronic state, the rotational distributions for $v' = 0$ are somewhat cold, peaking at rotational quantum numbers $j' = 5-7$ and reaching maximum values at $j' \approx 10$–12. For $v' = 1$, the rotational distributions show a similar trend, but with a significantly smaller cross section.

The sum over initial and final electronic states gives similar results in the two representations. This indicates that for this reaction the state-to-state integral cross sections do not show a clear evidence of nonadiabatic dynamics. It has been shown above that this reaction shows nonadiabatic effects only for very state-resolved reaction probabilities. Thus, we conclude that the only way these nonadiabatic effects could be investigated experimentally would be through the measurement of state-to-state differential cross sections.

Considering the good performance of the CS approximation discussed in Sec. III A (see Figure 3), we have studied the effect of the initial rovibrational state of the HF reagent on reactivity by using the *J*-shifting approximation[32] for the $O(^3P)+HF(v = 0, 1, 2)$ reactions. Figure 10 shows the comparison between the "exact" integral cross sections as a function of total energy for the reaction with $v = 0$ obtained in the adiabatic $1^3A''$ surface with those obtained for the same reaction but using the *J*-shifting approximation, with a rotational constant of $\approx 0.2\ cm^{-1}$ consistent with the transition state geometry. Given the good agreement found between them, we

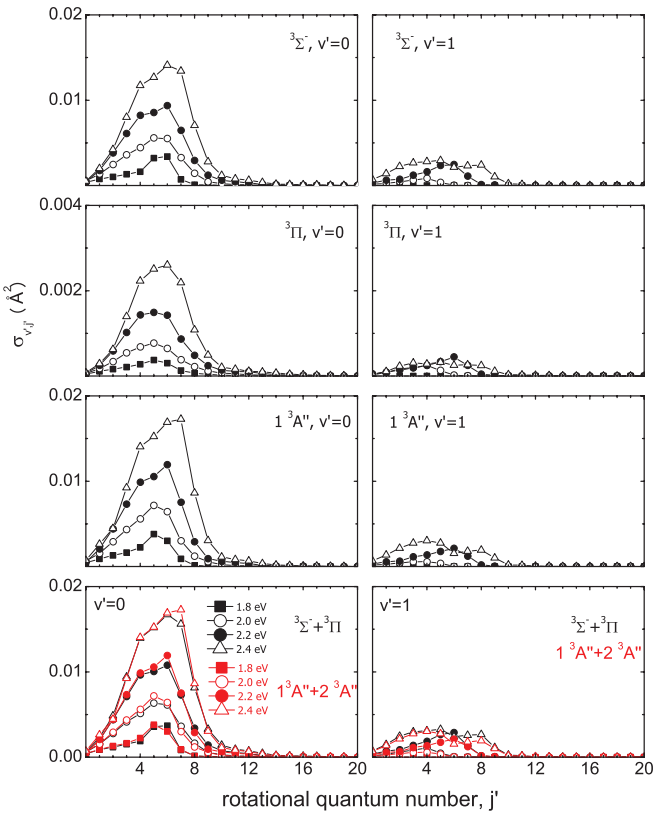

FIG. 9. Product rotational distributions for the $O(^3P)$+HF($v = 0, j = 0$)→OH(v', j')+F reaction at selected collision energies: 1.8 eV (black squares), 2.0 eV (open circles), 2.2 eV (black circles), and 2.4 eV (open triangles), for the adiabatic $1^3A''$ and $2^3A''$ states and for the diabatic $^3\Sigma^-$ and $^3\Pi$ coupled states as indicated. In the diabatic states, the cross sections for the two possible final electronic states have been added.

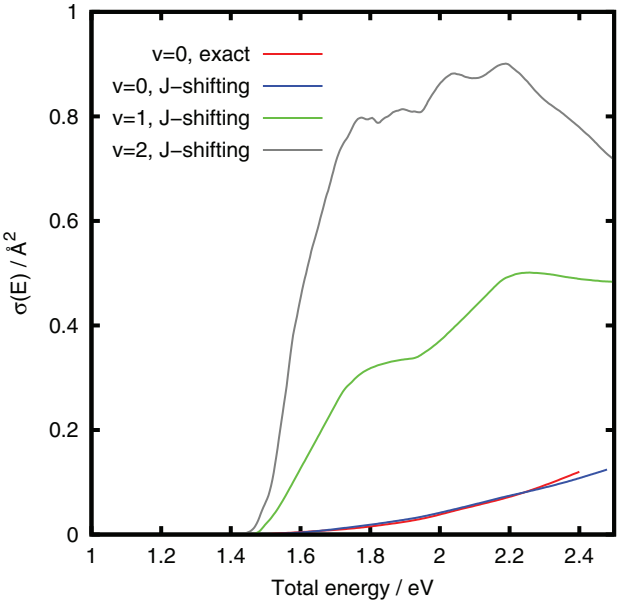

FIG. 10. Total integral cross section as a function of the total energy for the $O(^3P)$+HF($v = 0,1,2, j = 0$) reaction. Exact CC calculations for $v = 0$ (red). J-shifting calculations for $v = 0$ (blue), $v = 1$ (green), and $v = 2$ (grey). Notice the very good agreement between the exact CC and J-shifting calculations for $v = 0$.

conclude that the study of the effect of the reagent quantum state on the total reaction cross section can be studied properly using this approximation. We have found that HF($v = 0$) rotational excitation produces small enhancement/reduction of the integral cross section depending on the particular rotational j state considered, but the effect is not very important. The effect of HF vibrational excitation is by far more important, as can be seen in Figure 10. Reaction cross sections at the same total energy, i.e., collisional plus HF vibrational energy, increases considerably with v. This is a consequence of the late barrier character of the PES used, as predicted by Polanyi rules.[33–35]

IV. CONCLUSIONS

The $O(^3P)$+HF($v = 0, j = 0$)→OH($^2\Pi$)+F(^2P) reaction at hyperthermal collision energies has been studied using an exact time-dependent wave packet method in a coupled electronic diabatic representation to account for the nonadiabatic dynamics. The results have been compared with those obtained in the adiabatic representation. It is seen that for $J = 0$, the total and vibrationally state-resolved reaction probabilities obtained in the diabatic and adiabatic representation are nearly identical. In contrast, the rotationally state-resolved reaction probabilities show a clear dependence on the representation chosen, and this is taken as an evidence of nonadiabatic dynamics. However, after partial wave averaging to obtain total and state-to-state integral cross sections, these differences disappear in the rotationally state-resolved cross sections. This situation differs from that found for the reverse reaction, in which there is a noticeable increase of the reaction cross section in the diabatic representation.[27] In the present case, this is attributed to the fast dynamics at the high collision energies necessary to undertake this endoergic reaction. For the same reason, the spin-orbit splittings in the entrance channel have a negligible effect, in contrast again to the reverse reaction, where their inclusion changed the electronic partition function, yielding an increase of the rate constants. We conclude that nonadiabatic effects in this reaction are only expected to manifest in the state-to-state differential cross sections.

The collision energy dependence of the total and state-to-state integral cross sections shows a monotonous increase after threshold, which is a typical situation for a reaction with a large barrier. The CS approximation has been checked, showing a very good agreement with the exact CC calculations. In this reaction, the main axis of inertia is approximately parallel to the O-F axis, also very close to the **R** Jacobi vector describing either the reactant or product channels. Since the dynamics is rather direct and fast, the Coriolis couplings are not efficient, explaining why the CS approach is so well-adapted in this case.

The J-shifting approach provides also rather good results for the title reaction. This approximation has been used to study the influence of rovibrational excitation of the HF reagent on reactivity. It is found that reagent rotation has only a minor effect. On the contrary, reagent vibrational excitation produces a significant enhancement of the reactivity. This is

due to the late barrier character of the potential surface of this reaction.

ACKNOWLEDGMENTS

This work has been supported by the Spanish Ministerio de Ciencia e Innovación under Grant Nos. CSD2009-00038 (programa CONSOLIDER-INGENIO 2010 "Molecular Astrophysics: the Herschel and Alma era"), FIS2011-29596-C02, and CTQ2008-02578, and by Comunidad Autónoma de Madrid (CAM) under Grant No. S-0505/MAT/0303. We also acknowledge for a grant for computer time at CESGA computers. Partial financial support from the Scientific and Technological Research Council of TURKEY (TUBITAK) (Project No. TBAG-109T447) is gratefully acknowledged. Some computations have also been done on the High Performance and Grid Computing Center (TR-Grid) at ULAKBIM/TURKEY.

[1]D. Hastings and H. Garrett, "*Spacecraft-Environment Interactions*" (Cambridge University Press, 1996).
[2]E. Murad, J. Spacecr. Rockets **33**, 131 (1996).
[3]A. L. Brunsvold, H. P. Upadhyaya, J. Zhang, R. Cooper, T. K. Minton, M. Braunstein, and J. W. Duff, J. Phys. Chem. A **112**, 2192 (2008).
[4]A. L. Brunsvold, J. M. Zhang, H. P. Upadhyaya, T. K. Minton, J. P. Camden, J. T. Paci, and G. C. Schatz, J. Phys. Chem. A **111**, 10907 (2007).
[5]J. Zhang, J. P. Camden, A. L. Brunsvold, H. P. Upadhyaya, T. K. Minton, and G. C. Schatz, J. Am. Chem. Soc. **130**, 8896 (2008).
[6]J. P. Camden, R. Dawes, and D. L. Thompson, J. Phys. Chem. A **113**, 4626 (2009).
[7]A. J. Binder, R. Dawes, A. W. Jasper, and J. P. Camden, J. Phys. Chem. Lett. **1**, 2940 (2010).
[8]J. Zhang, A. L. Brunsvold, H. P. Upadhyaya, T. K. Minton, J. P. Camden, S. Garashchuk, and G. C. Schatz, J. Phys. Chem. A **114**, 4905 (2010).
[9]M. Tagawa, K. Yokota, K. Kishida, A. Okamoto, and T. K. Minton, ACS Appl. Mater. Interface **2**, 1866 (2010).
[10]J. M. Zhang, D. J. Garton, and T. K. Minton, J. Chem. Phys. **117**, 6239 (2002).
[11]B. H. Wu, J. M. Zhang, T. K. Minton, K. G. McKendrick, J. M. Slattery, S. Yockel, and G. C. Schatz, J. Phys. Chem. C **114**, 4015 (2010).
[12]J. P. Camden and G. C. Schatz, J. Phys. Chem. A **110**, 13681 (2006).
[13]S. Gómez-Carrasco, L. González-Sánchez, A. Aguado, O. Roncero, M. L. Hernández, J. M. Alvariño, and M. Paniagua, J. Chem. Phys. **121**, 4605 (2004).
[14]S. Gómez-Carrasco, O. Roncero, L. González-Sánchez, M. L. Hernández, J. M. Alvariño, M. Paniagua, and A. Aguado, J. Chem. Phys. **123**, 114310 (2005).
[15]S. Gómez-Carrasco, A. Aguado, M. Paniagua, and O. Roncero, J. Photochem. Photobiol. A **190**, 145 (2007).
[16]S. Gómez-Carrasco, L. González-Sánchez, A. Aguado, M. Paniagua, O. Roncero, M. L. Hernández, and J. M. Alvariño, Chem. Phys. Lett. **383**, 25 (2004).
[17]L. Gónzalez-Sanchez, S. Gómez-Carrasco, A. Aguado, M. Paniagua, M. L. Hernández, J. M. Alvariño, and O. Roncero, Mol. Phys. **102**, 2381 (2004).
[18]F. Gogtas, J. Comput. Chem. **29**, 1889 (2008).
[19]T. S. Chu, H. Zhang, S. Yuan, A. Fu, H. Si, F. Tian, and Y. Duan, J. Phys. Chem. A **113**, 3470 (2009).
[20]J. Zhao, Y. Xu, D. Yue, and Q. Meng, Chem. Phys. Lett. **471**, 160 (2009).
[21]T. Chu, J. Comput. Chem. **31**, 1385 (2010).
[22]Y. Xu, J. Zhao, D. Yue, H. Liu, X. Zheng, and Q. Meng, Chin. Phys. B **18**, 5308 (2009).
[23]L. Gónzalez-Sanchez, S. Gómez-Carrasco, A. Aguado, M. Paniagua, M. L. Hernández, J. M. Alvariño, and O. Roncero, J. Chem. Phys. **121**, 309 (2004).
[24]L. Gónzalez-Sanchez, S. Gómez-Carrasco, A. Aguado, M. Paniagua, M. L. Hernández, J. M. Alvariño, and O. Roncero, J. Chem. Phys. **121**, 9865 (2004).
[25]N. Elghobashi and L. González, Phys. Chem. Chem. Phys. **6**, 4071 (2004).
[26]S. Gómez-Carrasco, A. Aguado, M. Paniagua, and O. Roncero, J. Chem. Phys. **125**, 164321 (2006).
[27]A. Zanchet, T. González-Lezana, A. Aguado, S. Gómez-Carrasco, and O. Roncero, J. Phys. Chem. A **114**, 9733 (2010).
[28]C. D. Walter and H. G. Wagner, Ber. Bunsenges. Phys. Chem. **87**, 403 (1983).
[29]F. Rebentrost and W. A. Lester, J. Chem. Phys. **64**, 3879 (1976).
[30]A. Zanchet, O. Roncero, T. González-Lezana, A. Rodríguez-López, A. Aguado, C. Sanz-Sanz, and S. Gómez-Carrasco, J. Phys. Chem. A **113**, 14488 (2009).
[31]S. Gómez-Carrasco and O. Roncero, J. Chem. Phys. **125**, 054102 (2006).
[32]J. M. Bowman, Adv. Chem. Phys. **61**, 115 (1985).
[33]J. C. Polanyi and W. H. Wong, J. Chem. Phys. **51**, 1439 (1969).
[34]M. H. Mok and J. C. Polanyi, J. Chem. Phys. **51**, 1451 (1969).
[35]R. D. Levine and R. B. Bernstein, *Molecular Reaction Dynamics and Chemical Reactivity* (Oxford University Press, 1987).